

NASA/TM—2005-213433



Preparation and Analysis of Platinum Thin Films for High Temperature Sensor Applications

John D. Wrbanek
Glenn Research Center, Cleveland, Ohio

Kimala L.H. Laster
Akima Corporation, Brook Park, Ohio

The NASA STI Program Office . . . in Profile

Since its founding, NASA has been dedicated to the advancement of aeronautics and space science. The NASA Scientific and Technical Information (STI) Program Office plays a key part in helping NASA maintain this important role.

The NASA STI Program Office is operated by Langley Research Center, the Lead Center for NASA's scientific and technical information. The NASA STI Program Office provides access to the NASA STI Database, the largest collection of aeronautical and space science STI in the world. The Program Office is also NASA's institutional mechanism for disseminating the results of its research and development activities. These results are published by NASA in the NASA STI Report Series, which includes the following report types:

- **TECHNICAL PUBLICATION.** Reports of completed research or a major significant phase of research that present the results of NASA programs and include extensive data or theoretical analysis. Includes compilations of significant scientific and technical data and information deemed to be of continuing reference value. NASA's counterpart of peer-reviewed formal professional papers but has less stringent limitations on manuscript length and extent of graphic presentations.
- **TECHNICAL MEMORANDUM.** Scientific and technical findings that are preliminary or of specialized interest, e.g., quick release reports, working papers, and bibliographies that contain minimal annotation. Does not contain extensive analysis.
- **CONTRACTOR REPORT.** Scientific and technical findings by NASA-sponsored contractors and grantees.

- **CONFERENCE PUBLICATION.** Collected papers from scientific and technical conferences, symposia, seminars, or other meetings sponsored or cosponsored by NASA.
- **SPECIAL PUBLICATION.** Scientific, technical, or historical information from NASA programs, projects, and missions, often concerned with subjects having substantial public interest.
- **TECHNICAL TRANSLATION.** English-language translations of foreign scientific and technical material pertinent to NASA's mission.

Specialized services that complement the STI Program Office's diverse offerings include creating custom thesauri, building customized databases, organizing and publishing research results . . . even providing videos.

For more information about the NASA STI Program Office, see the following:

- Access the NASA STI Program Home Page at <http://www.sti.nasa.gov>
- E-mail your question via the Internet to help@sti.nasa.gov
- Fax your question to the NASA Access Help Desk at 301-621-0134
- Telephone the NASA Access Help Desk at 301-621-0390
- Write to:
NASA Access Help Desk
NASA Center for AeroSpace Information
7121 Standard Drive
Hanover, MD 21076

NASA/TM—2005-213433



Preparation and Analysis of Platinum Thin Films for High Temperature Sensor Applications

John D. Wrbanek
Glenn Research Center, Cleveland, Ohio

Kimala L.H. Laster
Akima Corporation, Brook Park, Ohio

National Aeronautics and
Space Administration

Glenn Research Center

January 2005

Acknowledgments

The authors are indebted to Dr. Liang-Yu Chen, Ohio Aerospace Institute (OAI), for his help in the adhesion testing. We would like to thank Drago Androjna, Akima Corporation, for the SEM pictures and Dorothy Lukco, QSS Group, Inc., for the XPS analysis of the films. We also would like to thank Gus Fralick, Sensors and Electronics Branch, for his review and comments on this paper. This work was sponsored at the NASA Glenn Research Center by the Engineering Capabilities Development Project of the Next Generation Launch Technology (NGLT) Program, the Alternate Fuel Foundation Technologies Subproject of the Low Emissions Alternative Power (LEAP) Project, and the Non-Destructive Evaluation (NDE) Program of the Office of Safety and Mission Assurance.

Trade names or manufacturers' names are used in this report for identification only. This usage does not constitute an official endorsement, either expressed or implied, by the National Aeronautics and Space Administration.

This work was sponsored by the Low Emissions Alternative Power Project of the Vehicle Systems Program at the NASA Glenn Research Center.

Available from

NASA Center for Aerospace Information
7121 Standard Drive
Hanover, MD 21076

National Technical Information Service
5285 Port Royal Road
Springfield, VA 22100

Available electronically at <http://gltrs.grc.nasa.gov>

Preparation and Analysis of Platinum Thin Films for High Temperature Sensor Applications

John D. Wrbanek
National Aeronautics and Space Administration
Glenn Research Center
Cleveland, Ohio 44135

Kimala L.H. Laster
Akima Corporation
Brook Park, Ohio 44142

Abstract

A study has been made of platinum thin films for application as high temperature resistive sensors. To support NASA Glenn Research Center's high temperature thin film sensor effort, a magnetron sputtering system was installed recently in the GRC Microsystems Fabrication Clean Room Facility. Several samples of platinum films were prepared using various system parameters to establish run conditions. These films were characterized with the intended application of being used as resistive sensing elements, either for temperature or strain measurement. The resistances of several patterned sensors were monitored to document the effect of changes in parameters of deposition and annealing. The parameters were optimized for uniformity and intrinsic strain. The evaporation of platinum via oxidation during annealing over 900 °C was documented, and a model for the process developed. The film adhesion was explored on films annealed to 1000 °C with various bondcoats on fused quartz and alumina. From this compiled data, a list of optimal parameters and characteristics determined for patterned platinum thin films is given.

Introduction

As part of NASA's mission to develop critical technologies that enable safer and more fuel efficient vehicles for aeronautics and space transportation, and to enable capabilities for long duration, more distant human and robotic missions for the Vision for Space Exploration, the Sensors and Electronics Branch of the NASA Glenn Research Center (GRC) has an effort to develop thin film sensors for surface measurement in propulsion system research. The sensors include those for strain, temperature, heat flux, and surface flow. The current challenges of the thin film sensor technology are to further develop electronics packaging and component testing of specialized sensors, further develop fabrication techniques on curves and complex surfaces, improve leadwire and film durability, and to address needs for higher temperature applications exceeding 1000 °C.

In 2002, a new sputtering system was purchased by NASA GRC from AJA International of North Scituate, Massachusetts under contract NAS3-01172 for the purpose of supporting research at GRC in the areas of high-temperature sensors and thin film micro-electro-mechanical systems (MEMS). The delivered system, an ATC2000 Sputtering System (#AJA1825) shown in figure 1, has three 3 inch (7.62 cm) diameter magnetron sources supplied with DC, pulsed DC, and RF power. Films can be deposited in an argon atmosphere, or in an atmosphere composed of a mixture of argon, oxygen, and/or nitrogen. The deposition system has the capability to deposit films onto substrates cooled to 10 °C to prevent the overheating of the photoresist used in photolithographic processes, and it also has the capability to heat the substrate to 600 °C to form a crystalline structure for depositing ceramics. The accuracy and longevity of the sensors at high temperatures are also dependent on the purity of the films that are deposited, such that an ultrahigh vacuum (UHV) deposition system was required. To improve the throughput of the different types of sensor designs, a loadlock was installed on the main chamber to shorten pumpdown time and to preserve the purity of the system. The system has the capability for the



Figure 1.—The deposition chamber, load lock, and computer interface of the ATC2000 Sputtering System (#AJA1825).

depositions to occur with adjustable, well-controlled conditions via an automatic control system for reproducible results.

The most important near-term application of this system is the development of durable high-temperature thin film sensors. The sensors will be composed of a variety of materials, from metals such as platinum and palladium-chrome alloys, to ceramics such as alumina. These materials, configured in a variety of multi-layer structures, need to be investigated to determine the optimum structure for the sensors.

Platinum Sensor Samples

Besides its decorative value as a corrosion-resistant precious metal, platinum's usefulness in thermometers, electrodes, and catalysts is well known (ref. 1). Thin platinum films have long been used as thermocouple elements in the aeronautical research field (ref. 2), as well as resistance thermometers (ref. 3) and strain gauges (ref. 4). In the biomedical community, ultra-thin platinum films are seen as a useful conductive biocompatible material, and applications are being explored in coronary artery stents, auditory prostheses, and pace-maker electrodes (ref. 5). Therefore, establishing preparation parameters using platinum films with the new system would have immediate applications.

Since an application of the platinum films in NASA's thin film sensor research would be as a resistive-based sensor, the studies were carried out by depositing films in a resistive strain gauge pattern and making measurements of the resistance with an ohmmeter. The strain gauge pattern, shown in figure 2, has an active area of 1.5×1.2 mm and an element trace length to width ratio (l/w) of 250. On each sample, the gauges were patterned in a 5 column by 3 row array with column spacing of 5 mm and row spacing of 15 mm on a $5 \text{ cm} \times 3.8 \text{ cm} \times 1 \text{ mm}$ ($2 \times 1.5 \times 0.040$ inch) alumina substrate. This gives an effective area studied of 2.15×3.12 cm, or 6.7 cm^2 . Invariably, orientation of the patterns on the sample allowed measurements of only 14 gauges on each sample.

The deposition runs used a lift-off process developed at NASA GRC (ref. 6). A schematic of the process steps is given in figure 3 (ref. 4). After cleaning with soap and DI water, the cut alumina substrates were rinsed in acetone and then in methanol. A thin layer of copper was deposited on the substrate as a sacrificial layer. The photolithography was performed by spin-applying photoresist on the copper and soft-baked at $90 \text{ }^\circ\text{C}$ for 60 seconds. The strain gauge pattern was exposed, developed, and then hard-baked for 30 minutes. The exposed pattern was etched with nitric acid and water. The substrate was placed on the $10 \text{ }^\circ\text{C}$ -cooled substrate holder in the sputtering system 1 hour before the deposition of platinum at the desired parameters. After the deposition, the photoresist was dissolved and the remaining

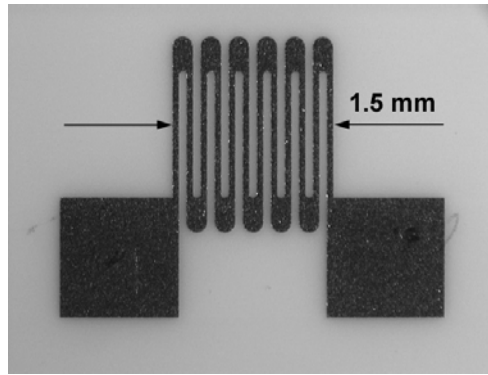


Figure 2.—Strain gauge pattern used in these studies.

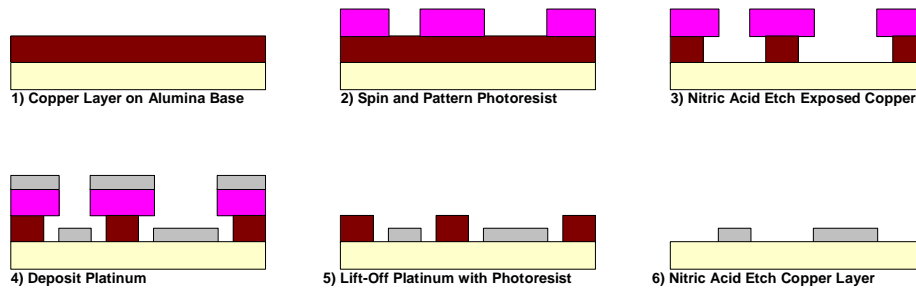


Figure 3.—Lift-off Process used in constructing the strain gauge patterns (refs. 4 and 6).

copper etched off with the nitric acid. The completed sample was rinsed in DI water and blown-dry with nitrogen.

In the first three minutes of the deposition of platinum, a reactively sputtered platinum oxide was deposited as an adhesion layer. This adhesion layer is commonly used at GRC based on work done for NASA at UCLA (refs. 2 and 7), and is used elsewhere for platinum electrodes on ferroelectric oxides (refs. 8, 9, and 10).

Pressure Optimization

The first runs were conducted to determine the optimal system pressure for the depositions through optimizing the film resistivity, uniformity, and deposition rate. The samples were produced with parameters based on experience with an older diode sputtering system also at the GRC Microsystems Fabrication Clean Room Facility. Five runs total were performed covering the pressure range 1 mTorr to 8 mTorr, and a summary is given in table 1. The sample numbers given are the month and day of fabrication completion (mdd). The films were deposited with 100 W DC (2.2 W/cm²) using a 3 minute bond coat and a 1 hour final coat. The gas mix used had an Argon/Oxygen ratio of 30/20 for the bond coat, and pure Argon for the final coat. The resistivity (ρ) was determined from the average measured resistance (R), the film thickness (h), and the sensor pattern's length to width ratio (l/w):

$$\rho = R \cdot h / \frac{l}{w} \quad (1)$$

The film thickness was measured on a Dektak profilometer with a precision of $\pm 0.1 \mu\text{m}$, and the resistances were measured on a Fluke multimeter with the precision of $\pm 0.2 \Omega$.

TABLE 1.—PRESSURE OPTIMIZATION SAMPLES

Sample (<i>mmd</i>)	Deposition System Pressure (mTorr)	Average Current (mA) at 100 W	Film Thickness (μm) ($\pm 0.10\mu\text{m}$)	As-Deposited		4 hr 1000 °C Anneal		8 hr 1000 °C Anneal	
				Resistivity ($\mu\Omega\text{-cm}$)	Film Uniformity	Resistivity ($\mu\Omega\text{-cm}$)	Film Uniformity	Resistivity ($\mu\Omega\text{-cm}$)	Film Uniformity
0128	1	239.4	0.72	14.3	3.1%	10.4	3.2%	11.4	4.9%
0131	3	272.8	0.74	15.5	2.0%	11.1	1.9%	11.5	2.1%
0121	4	275.7	0.72	16.8	0.7%	11.8	0.5%	12.1	0.9%
0130	5	279.5	0.74	16.1	2.0%	11.2	1.9%	11.6	2.1%
0117	8	280.4	0.80	17.9	1.8%	11.5	1.1%	11.7	1.3%

Despite the low accuracy of the resistivity due to the large uncertainty in film thickness, the relative precision of the measurements on each sample is valid to ± 0.6 percent based on the resistances that varied between 35 and 60 ohms. The reported film uniformity is the standard deviation of the measurements for that sample divided by the average resistance. In this regard, the uniformity is not only a measurement of the uniformity of the film thickness, but the uniformity of the film resistivity as well.

Based on our standard treatment for annealing (ref. 2), the film samples were annealed in air at 1000 °C for 4 hours. This was done twice to give data on film resistivity for as-deposited, 4 and 8 hours annealed.

From the measured film thickness, the pressure affects film deposition rate approximately:

$$Rate[\mu\text{m/hr}] = 0.70\mu\text{m/hr} + 0.011\mu\text{m/hr/mTorr} * Pressure[\text{mTorr}] \quad (2)$$

This relation (2) is shown graphically in figure 4. The current generated by the plasma is shown in figure 5 for platinum and platinum oxide films. The current maximized after 5 mTorr for pure platinum, 4 mTorr for platinum oxide films. Film uniformity of the annealed films is minimized near 1 percent for pressures greater than 4 mTorr as shown in figure 6. Uniformity degrades as the pressure drops for pressures under 4 mTorr. It is not apparent how the uniformity is affected by annealing. From these runs, the optimal pressure for the deposition of platinum films to minimize uniformity and maximize deposition rate is 5 mTorr, and 4 mTorr for the platinum oxide.

As seen in figure 7, the resistivity of the as-deposited films is increased by increasing deposition pressure, suggesting the increase of intrinsic stresses by the quenching of surface mobility of the depositing film by the gas. Annealing the films reduced the resistivity closer to bulk values for all the samples. However, annealing with increasing time increased the observed resistivity. This effect, though initially surprising, was found to be reported previously, but without explanation (ref. 9). One possible reason for the change is the evaporation of the platinum films through volatile oxidation while annealing, which was demonstrated and quantified in the subsequent runs described below.

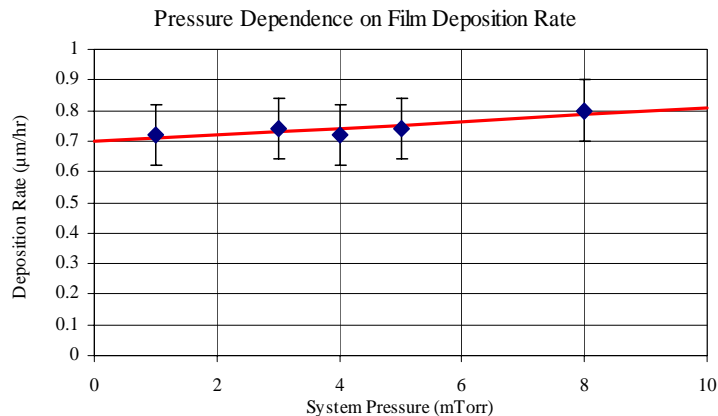


Figure 4.—Deposition Rate vs. System Pressure with fit to data.

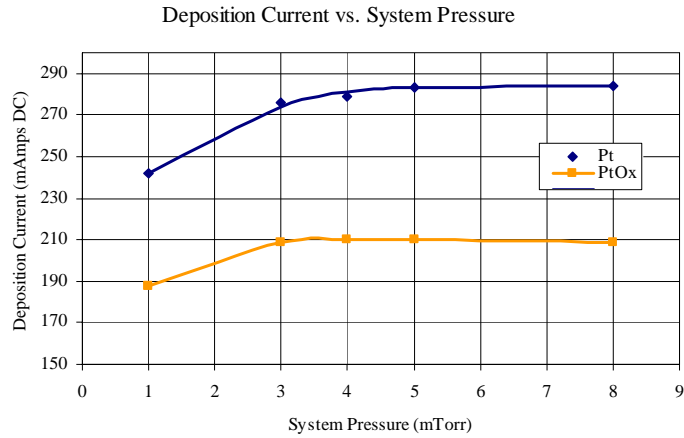


Figure 5.—Deposition Current vs. System Pressure. The lines are included to guide the eye.

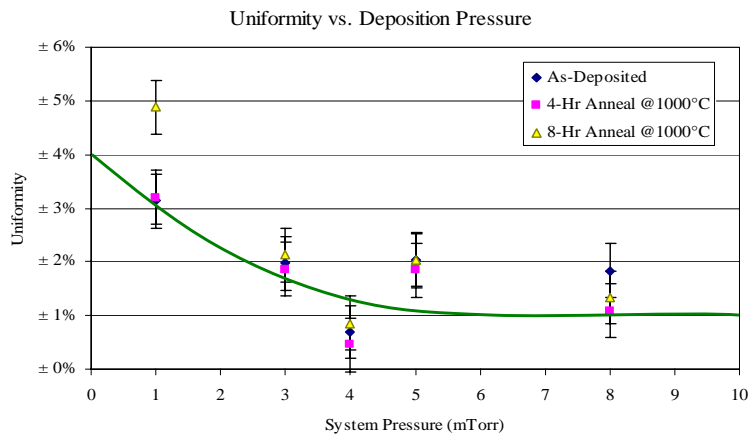


Figure 6.—Film Uniformity vs. System Pressure. The curve is included to guide the eye.

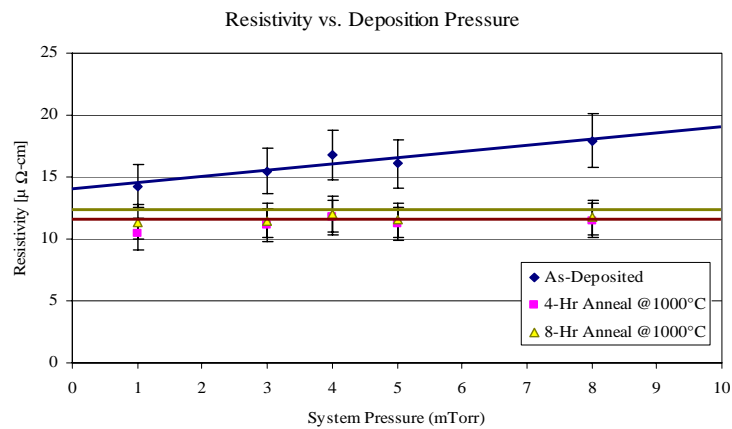


Figure 7.—Film Resistivity vs. System Pressure. The lines are included to guide the eye showing the as-annealed resistivity trend, 4 hour anneal trend, and 8 hour anneal trend.

Power Optimization

To determine the optimal power settings for film deposition, several samples were produced using the system pressure of 5 mTorr based on the results of the preceding section to examine the effect of the magnetron source power on the depositions. The magnetron was set at a power such that all of the runs covered the range of 25 to 300 W DC, and the time-averaged delivered power and current was recorded for each run. To give an indication of the role of self-annealing during deposition, these samples were not cooled. A summary is given in table 2 below.

TABLE 2.—POWER OPTIMIZATION SAMPLES

Sample (mmdd#n)	Average Power (Watts DC)	Average Current (mA)	As-Deposited		Post-Anneal		Fractional Change in Resistance
			Usable sensors	Resistance (ohms)	Resistance (ohms)	Calculated Thickness (μm)	
1208#1	28.5	82.5	94%	371.4	OPEN	<0.03	-
1208#2	52.3	146.3	100%	133.2	153.5	0.172	-
1208#8	76.1	209.4	100%	78.5	50.9	0.519	0.54
1208#3	99.0	260.6	100%	54.2	36.4	0.727	0.49
1208#4	146.6	363.5	83%	31.9	24.2	1.095	0.32
1208#5	194.2	462.6	21%	22.2	16.5	1.60	0.35
1208#6	241.9	554.1	61%	19.1	14.1	1.87	0.35
1208#7	289.5	651.2	79%	14.0	11.7	2.27	0.21

The resistances of the samples were measured before and after being annealed in the air furnace. Based on the results of the annealing of the films shown in figure 7, the annealing of the samples at 1000 °C for 4 hours was considered to result in the films having bulk resistivity. The thicknesses of the films were determined by using the bulk resistivity for platinum of $\rho = 10.58 \mu\text{Ohm-cm}$ and $l/w = 250$ for the sensor pattern. The accuracies of the resulting thicknesses are dependent on the measured resistances and the uniformity of the film. The measurements on each sample gave standard deviations of ± 4 percent. A plot of thickness vs. current gives a slope of $4\mu\text{m/hr/Amp}$, as shown in figure 8. The plot also shows an -86mAmp offset of the current in determining the post-anneal thickness. Note the increasing resistances of samples 1208#1 and 1208#2 in table 2, which indicate possible film loss during annealing.

The power plotted against the current as measured in table 2 is shown in figure 9. The best fit of the plot is:

$$Power = 167 \text{ Ohms} * Current * (2 \text{ Amps} + Current) \quad (3a)$$

which can be approximated as:

$$Power = 0.464 \text{ W/mA} * (Current - 37.25 \text{ mA}) \quad (3b)$$

The best fit (3a) and the linear approximation (3b) are also shown in figure 9.

Since there was no cooling, the power input into the deposition allowed the self-annealing of the film to be more marked than without cooling. Figure 10 shows a plot of the fractional decrease of annealed resistance and the rate of film formation failure of the sensors vs. power, not including samples 1208#1 and 1208#2 where the resistance measurements due to film loss are most apparent. The best fit to the resistance data was found to be an inverse power (Watt^{-1}) relationship:

$$(R_{dep} - R_{bulk})/R_{bulk} = 58.5\text{W}/Power \quad (4)$$

Note that for 100 W, this fit (4) gives 0.585, slightly higher than the 0.52 from sample 0130 above. In table 3 below, three more samples were generated at these parameters with cooling with $(R_{dep} - R_{bulk})/R_{bulk}$ of 0.4 on average. The fit (4), then, appears to be accurate to ± 25 percent. However, the failure of the films to produce a complete set of usable sensors with powers above 100 W is indicative of stresses in film formation which cannot be ignored. This is roughly a linear trend of about 5 percent failures (1 sensor) per 17 W above 100 W, also accurate to ± 25 percent based on table 3 below.

This fractional change in resistance not due to film loss can be calculated for 1208#1 and 1208#2 to be 2.05 and 1.12 respectively, leading to a determination of their respective pre-anneal thickness of 0.124 and 0.335 μm . Using the difference of the pre- and post-anneal thicknesses from the fitted curves of 0.091 μm , the pre-anneal deposition rate can be deduced, which is overlaid on figure 8. This pre-anneal deposition plot indicates a 0.257 μm “negative” film thickness, corresponding to 64mAmps as the current for a zero deposition rate which reflects energy required for film growth. The rate can be stated in equation form for 5 mTorr pressure as:

$$\text{Rate } (\mu\text{m/hr}) = (\text{Current} - 64\text{mAmps}) * 4\mu\text{m/hr/Amp} \quad (5)$$

Note that the above relation (5) is affected by 0.011 $\mu\text{m/hr/mTorr}$ for changes in system pressure.

For the optimal power setting, higher powers give a higher deposition rate but powers of 100 W and lower allow minimal film formation failures, but increase the intrinsic stress of the film. Sample 1208#3 at the nominal 100 W setting gives the highest deposition rate as well as lowest fractional resistance change due to deposited stresses and minimal sensor failures for this range.

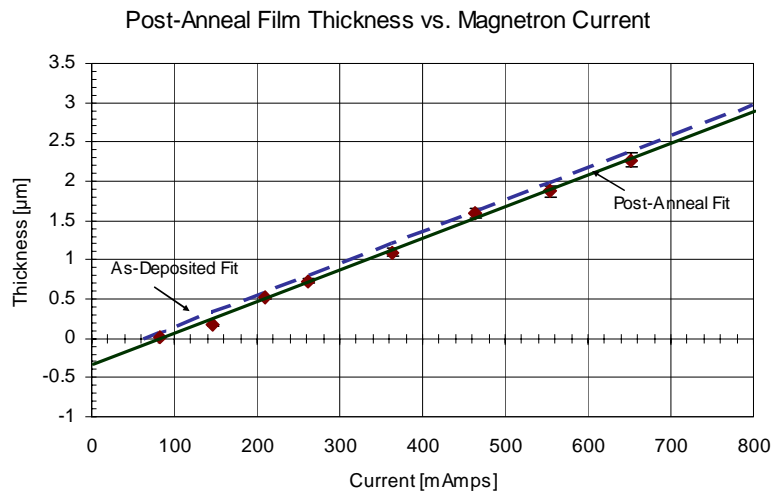


Figure 8.—Post-Anneal Film Thickness vs. Magnetron Current. The error bars indicate the ± 4 percent uncertainty from the standard deviation of the measured resistance. The solid line is the best fit for the data, and has a slope of 4.0 $\mu\text{m/hr/amp}$. The dashed line indicates the best fit shifted up 0.091 μm as the as-deposited thickness before annealing.

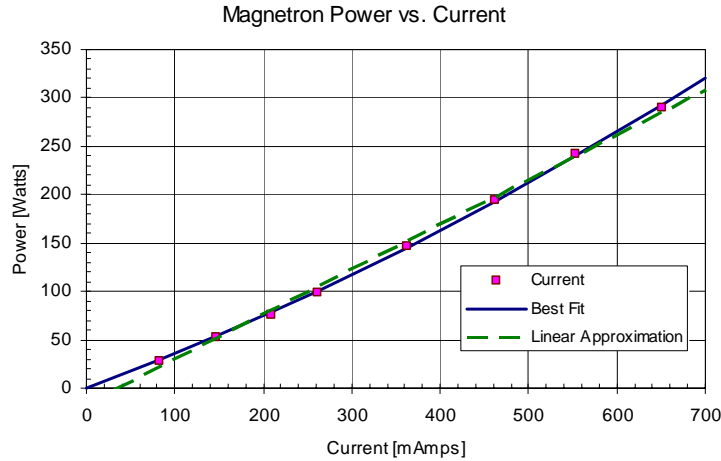


Figure 9.—Magnetron Power vs. Current. The best fit to the data and a linear approximation are shown as well.

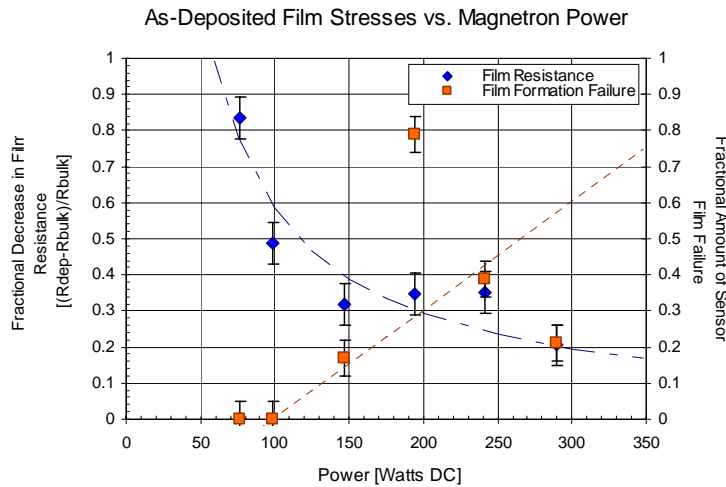


Figure 10.—Film Stresses for as-Deposited Film vs. Power. The two plots show the decrease in film resistance seen after annealing and the amount of film failure in deposition. The error bars indicate the ± 0.057 uncertainties in the measurement. Lines are provided to guide the eye.

Annealing Optimization

Annealing platinum prior to use, particularly as a resistive sensor, is standard practice in bulk platinum (refs. 1 and 11) and in films to relax intrinsic stresses due to misaligned islands or grains incorporated in the as-deposited films at low temperatures (refs. 2, 12, and 13). To determine the optimal annealing time and to determine the evaporation rate, three samples were fabricated using identical settings: The DC Power at 100 W using 5 mTorr system pressure, 3 minutes platinum deposition of a bond coat using Ar/O₂ = 40/4 gas flow followed by 1 hour deposition using pure argon. Based on the fit of figure 8 and the deposition current, the films were $0.77 \pm 0.05 \mu\text{m}$ thick. The samples had 14 useable elements on each coupon. The standard deviation of the as-annealed resistance was uniform to ± 2 percent on the samples, but ± 3 percent between coupons, which is an indication of a ± 2 percent variation in l/w due to the chemical etch. Each sample was annealed at a different temperature for 2 hours four times, then once for four hours, then once again for six. For additional data points, the sample 0130 from earlier was

annealed at 1000 °C for another 8 hours, and sample 0131 was annealed at 1100 °C three times for four hours to give a total of 12 hour annealing time at that temperature. The resistance was measured for these samples in the same fashion of the pressure optimization runs earlier, and the annealing rates were determined.

Intrinsic Stress Relaxing

To determine the rate of annealing of our films, we treat the relaxing of dislocations in the film as the primary process. The rate of relaxing of dislocations has been found to be proportional to the temperature and the intrinsic stress being relaxed (ref. 14). This intrinsic stress in a film is proportional to the observed change of resistivity of the film from bulk (ref. 12).

The average rate was determined using the resistance measurements from samples 0326#1–3 at anneal times $t = 2$ hours and $t = 4$ hours annealing for each sample. No estimate was made from samples 0130 since it showed considerable film loss, and an estimate of annealing rate could not be made without significant uncertainty. These rates are shown in table 3.

TABLE 3.—ANNEALING RATES

Sample (mmdd#n)	Annealing Temperature (±20 °C)	Initial Intrinsic Stress (E/K)	Annealing Rate at $t = 2$ hrs (hr ⁻¹)	Annealing Rate at $t = 4$ hrs (hr ⁻¹)	Average Annealing Rate (hr ⁻¹)	Rate from Least Squares Fit (hr ⁻¹)
0326#3	710	0.34	1.70	0.84	1.27	1.25
0326#2	810	0.38	1.67	1.26	1.46	1.48
0326#1	910	0.44	1.709	1.716	1.712	1.712

The intrinsic stress σ is proportional the intrinsic strain ϵ which is proportional to the change in resistance ΔR , and thus resistivity ρ assuming no change in the height of the film:

$$\sigma \frac{K}{E} = K\epsilon = \frac{\Delta R}{R} = \frac{R_{film} - R_{bulk}}{R_{bulk}} = \frac{\left(\frac{\rho}{h} \frac{L}{w}\right)_{film} - \frac{\rho}{h} \frac{L}{w}}{\frac{\rho}{h} \frac{L}{w}} = \frac{\rho_{film} - \rho}{\rho} \quad (6)$$

During annealing, the intrinsic stress and resistivity changes with time:

$$\frac{R_{film}(t) - R_{bulk}}{R_{bulk}} = \frac{\rho(t) - \rho}{\rho} = \frac{K}{E} \sigma_0 e^{-A(T, \sigma_0)t} \quad (7)$$

Here in (6) and (7), σ_0 is the initial intrinsic stress of the film, K is the strain sensitivity (gauge factor), E is Young's modulus, A is the rate, T the temperature, and t the time.

Linear fit of samples 0326#1–3 gives a temperature dependent rate A from the three film samples as:

$$A(T) = 0.002321 \text{ hr}^{-1} * (T - 172 \text{ °C}) \quad (8)$$

The fit (8) is also shown in table 3 and graphically in figure 11. This fit assumes an initial intrinsic stress of $0.40E/K$ for the three samples. Assuming that the rate is proportional to the initial intrinsic stress, we can restate the rate fit as:

$$A(T, \sigma_0) = 0.00580 \text{ hr}^{-1} * \left(\frac{K}{E} \sigma_0\right) * (T - 172 \text{ °C}) \quad (9)$$

Ideally, annealing for six times the inverse of this rate (9) will give the resistivity stable to one part in 1000 for an initial intrinsic stress of $0.5E/K$. However, we have found that the film thickness itself changes during annealing as well, which needs to be considered.

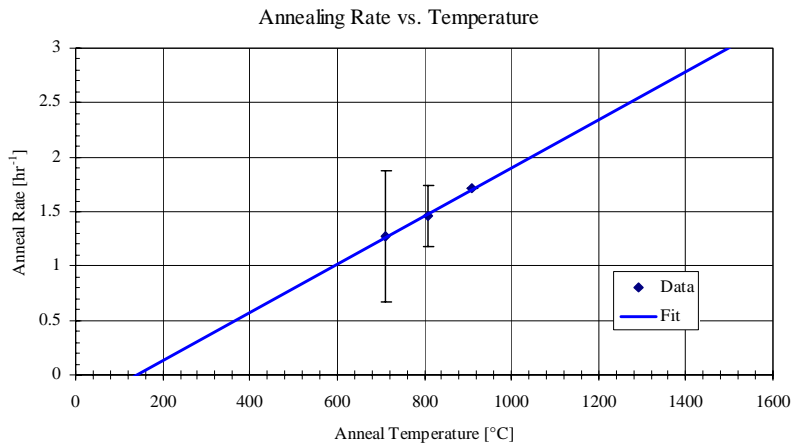


Figure 11.—Annealing Rate vs. Temperature. The line is a least-squares fit of the data points.

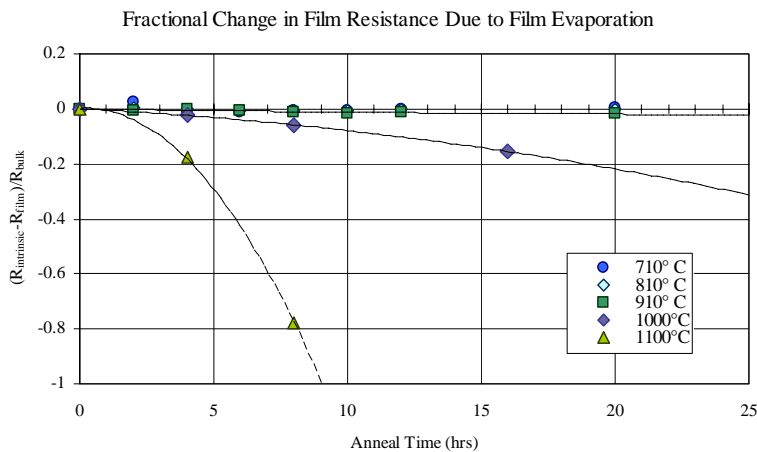


Figure 12.—Fractional Change in the Film Thickness vs. Annealing Time for various temperatures. The lines are to guide to eye for the 910, 1000, and 1100 °C annealing temperatures.

Film Loss

If the reduction of intrinsic stress predicted by the fit of the annealing rate is subtracted from the measured resistance of the film, a deviation is seen that can be explained by film loss during annealing. Figure 12 shows this difference as a fractional loss of film.

In order to test the robustness of the platinum films under annealing conditions, samples of the films with different platinum oxide bondcoats were fabricated on 1 inch (2.54 cm) square quartz (–QZ) and 1 inch (2.54 cm) square alumina (–AO) substrates, both 0.040 inch (1 mm) thick. Initially, the films were deposited nano-thin (<100 nm) to attempt to determine the composition after annealing. The deposition parameters for the nano-thin films are given in table 4. The film thickness is estimated from the average current and the deposition rate related in the above section. They were then annealed for 4 hours in air at 500, 700, and then 1000 °C, in parallel with the annealing studies conducted above.

No change was visible in the films after the 500 and 700 °C anneals, but much of the films were lost after the 1000 °C anneal, as shown in figure 13. A visual comparison of the as-deposited and post-anneal films for samples 0401#2 –QZ and –AO showing the evaporation is given in figure 14. The remaining hazy film did not pull off with a rudimentary “tape test” with transparent tape, indicating that the film failure was not due to delamination but reaction with the air. The estimated rate from this test is in the range of 120 to 200 Å/hr.

TABLE 4.—NANO-THIN FILM ADHESION SAMPLES

Sample #	3 min Bond Coat Gas Flow Mix (Ar/O ₂)	3 min Final Coat Gas Flow Mix (Ar/O ₂)	Average Current (mA) at 100 W	Est. Film Thickness (Å) (±176Å)
0401#1 -QZ and -AO	40/0	40/0	260	796
0401#2 -QZ and -AO	40/4	40/0	235	695
0401#3 -QZ and -AO	40/10	40/0	230	672
0401#4 -QZ and -AO	20/20	40/0	226	656

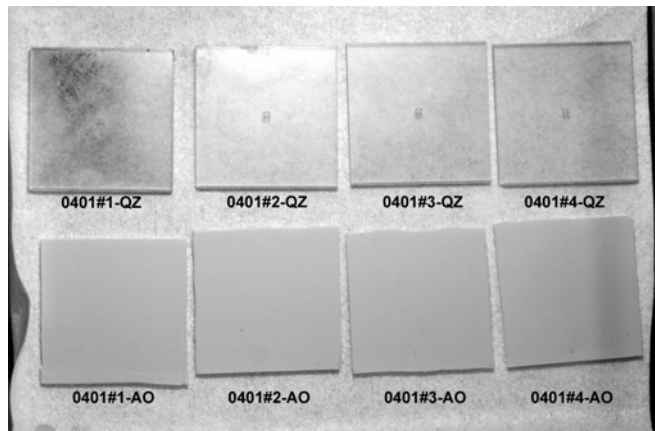


Figure 13.—Film loss in samples 0401#1–4 demonstrated after a 4 hr anneal at 1000 °C.

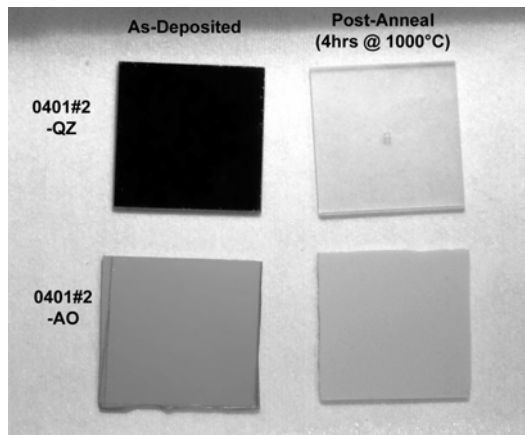


Figure 14.—Visual difference in nano-thin films before and after annealing for 4 hrs at 1000 °C with samples 0401#2 -QZ and -AO.

Unfortunately, direct measurement of the film loss was precluded because the instrumentation was not sensitive to the minute changes seen in this film loss. To quantify the film loss during annealing, the result of the above test was compared to the calculated film thickness decrease of the samples from other annealing tests. A least-squares fit of the result for each annealing temperature gives a fractional film thickness decrease per hour and the equivalent film loss rate as shown in table 5.

TABLE 5.—FILM LOSS RATE FOR VARIOUS ANNEALING TEMPERATURES

Sample (mmd#n)	Annealing Temperature (°C) (± 20 °C)	Fractional Film Thickness Decrease (per hour)	Equivalent Film loss rate (Å/hr)
0326#3	710	0.00013	4 ± 24
0326#2	810	0.00023	4 ± 23
0326#1	910	0.00106	9 ± 23
0130	1000	0.01203	57.4 ± 25
0131	1000	0.00806	66 ± 32
0401#4	1000	-	160 ± 40
0131	1100	0.05635	374 ± 45

The rate of film losses for samples 0326#1–#3 are within the uncertainty of the measurements, but they are not for samples 0130, 0131, and 0401#4, corresponding to temperatures above 900 °C. A model was pursued to determine the evaporation rate of the platinum films in air of our annealing furnace.

The film loss is assumed to be by the vaporization of platinum from the surface through reaction with oxygen. This volatility of platinum and other noble metals was studied at high temperature by Alcock and Hooper, who demonstrated that the oxidation reaction forms vaporous PtO_2 and determined the partial pressure of the oxide in air (ref. 15). The observed result is a net evaporation following:



Net mass flux due to evaporation is dependent on the difference between the partial pressures of the evaporating gas and the condensate at the temperature of the system. In a true evaporation, there is some amount of condensation of the vapor back on the surface, dependent on the partial pressure and the temperature of the surface. At temperatures greater than 600 °C, solid platinum oxide decomposes into solid platinum and gaseous oxygen (ref. 10). The balance of the mass lost due to the partial pressure of the vaporizing gas and the mass gained by the condensation of the gas on the surface gives the resulting mass flux from the surface J_{net} as:

$$J_{net} = \frac{1}{4} \alpha_m \nu (p_{gas} - p_{cond}) / RT \quad (11)$$

This relation is referred to as the Hertz-Langmuir-Marcelin-Knudsen equation (HLMK) expressed in terms of partial pressure (ref. 16). Here, α_m is a dimensionless accommodation coefficient (between 0 and 1), ν is the molecular velocity, p_{gas} is the partial pressure of the volatile gas, p_{cond} is the partial pressure of the condensing gas on the surface (fugacity), R is the gas constant, and T is the temperature.

For platinum oxide, the molecular velocity is:

$$\nu = \sqrt{\frac{8RT}{\pi M}} = \sqrt{\frac{8 * 8.3144 J / mol / K * T}{\pi * 0.227 kg / mol}} = 9.66 m / s / K^{1/2} * \sqrt{T} \quad (12)$$

Since the partial pressure of platinum oxide has been studied at high temperatures by Alcock and Hooper (ref. 15), we will use their value of $p_{gas} = 1216 \text{ Torr} * e^{-8585/T}$. The fugacity p_{cond} is proportional to the concentration of the condensate (c_{cond}) by Henry's Law ($p_{cond} = c_{cond}/H$; H = Henry's Law coefficient), and it is assumed the fugacity reaches some equilibrium during the evaporation. Using $R = 0.62363 \text{ m}^3 \text{ Torr mol}^{-1} \text{ K}^{-1}$:

$$J_{net} = 3.87 \text{ mol.K}^{1/2} / \text{m}^2 / \text{s} / \text{Torr} * \alpha_m (p_{gas} - p_{cond}) / \sqrt{T} \quad (13)$$

With platinum's molecular density of $8.78 \times 10^4 \text{ mol/m}^3$, we have an evaporation rate of:

$$B = 0.16K^{1/2} m / hr / Torr * \alpha_m (p_{gas} - p_{cond}) / \sqrt{T} \quad (14)$$

Using $p_{gas} = 1216 \text{ Torr} * e^{-8585/T}$, we can fit the data using α_m and p_{cond} as unknowns. The resulting fit with $\alpha_m = 7.46 \times 10^{-6}$ and $p_{cond} = 1.18 \text{ Torr}$ is shown in figure 15. From the fit, the onset of evaporation appears to be between 950 and 990 °C. By 1000 °C, the film loss is $0.0084 \text{ } \mu\text{m/hr}$. Also, at 1500 °C, the maximum short-term usable temperature for platinum thin films, the evaporation rate is predicated to be about $0.24 \text{ } \mu\text{m/hr}$. These rates are applicable to only our enclosed annealing furnace, and are considered valid to ± 48 percent due to the uncertainties of the fitted unknowns of the model. The rates are dependent on a number of factors including the test configuration and flow of air across the sample, and other applications may see rates an order of magnitude higher or lower than these (ref. 17).

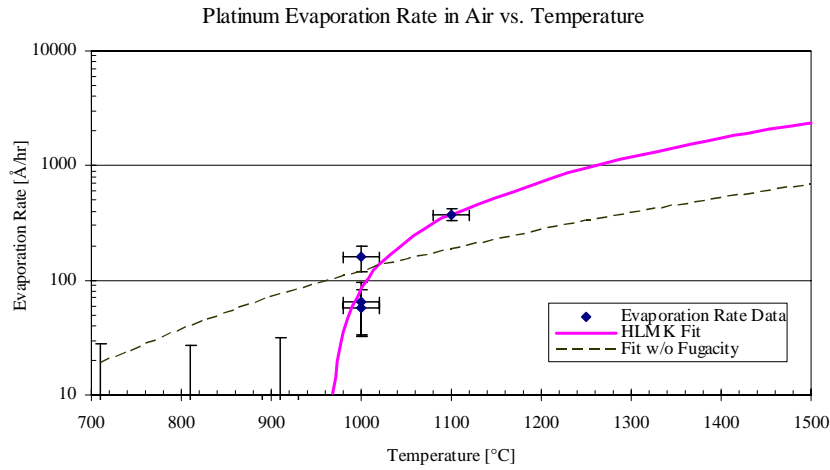


Figure 15.—Platinum Evaporation Rate vs. Air Anneal Temperature. The line is the resulting fit to the Hertz-Langmuir-Marcelin-Knudsen equation (HLMK). The dashed line shows the fit ignoring the condensation pressure of the evaporating platinum oxide (fugacity).

Net Effect of Annealing

The observed change in resistance from annealing can be expressed as:

$$\frac{\Delta R}{R} = \frac{R_{film}(t) - R_{bulk}}{R_{bulk}} = \frac{\frac{\rho(t)}{h(t)} \frac{l}{w} - \frac{\rho}{h} \frac{l}{w}}{\frac{\rho}{h} \frac{l}{w}} = \frac{\frac{\rho(t)}{\rho} - \frac{h(t)}{h}}{\frac{h(t)}{h}} \quad (15)$$

The resistivity change with time due to relaxing intrinsic stress is:

$$\rho(t) = \rho \left(1 + \left(\frac{K}{E} \sigma_0 \right) e^{-At} \right) \quad (16)$$

The initial resistance $\rho(1 + \frac{K}{E} \sigma_0)$ is 1.40ρ for samples 0326a–c. Sample 0130 has a higher initial resistance ($\rho(1 + \frac{K}{E} \sigma_0) = 1.52\rho$), but the target was changed between the pressure optimization runs and the annealing optimization runs, and this may reflect varying quality of the targets.

For the film thickness change due to evaporation:

$$h(t) = h\left(1 - \frac{B}{h}t\right) \tag{17}$$

The resulting change in resistance with time is:

$$\frac{R_{film}(t) - R_{bulk}}{R_{bulk}} = \frac{\left(\frac{K}{E} \sigma_0\right) e^{-At} + \frac{B}{h}t}{1 - \frac{B}{h}t} \tag{18}$$

This net effect is shown with the data points of samples in figures 16 to 19.

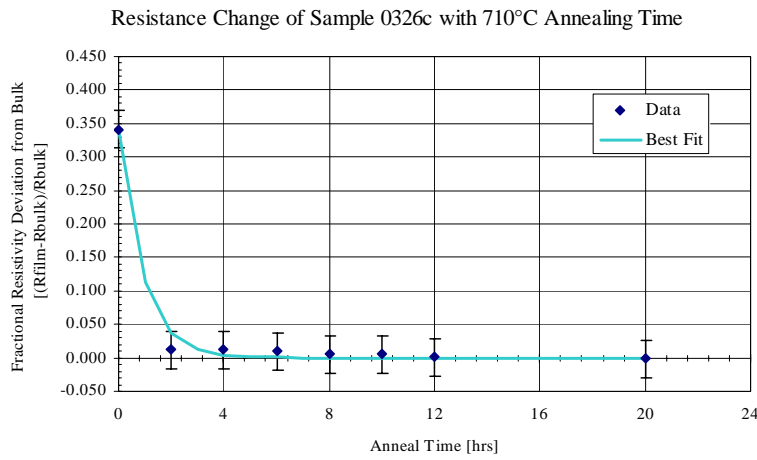


Figure 16.—Resistance change of sample 0326c showing data points and best fit from the developed model.

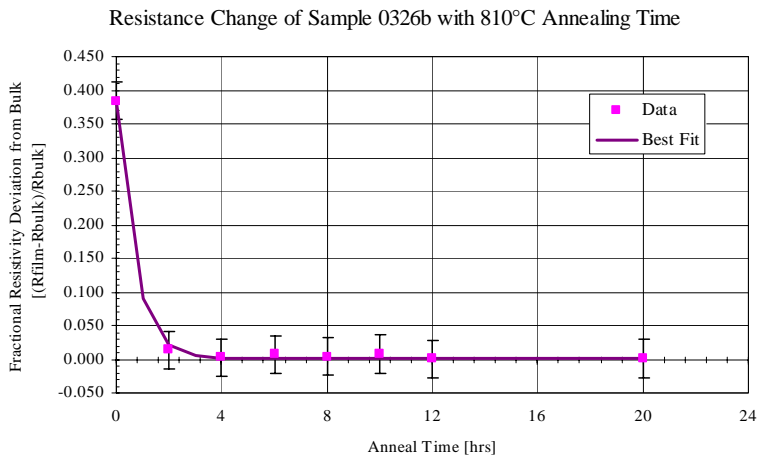


Figure 17.—Resistance change of sample 0326b showing data points and best fit from the developed model.

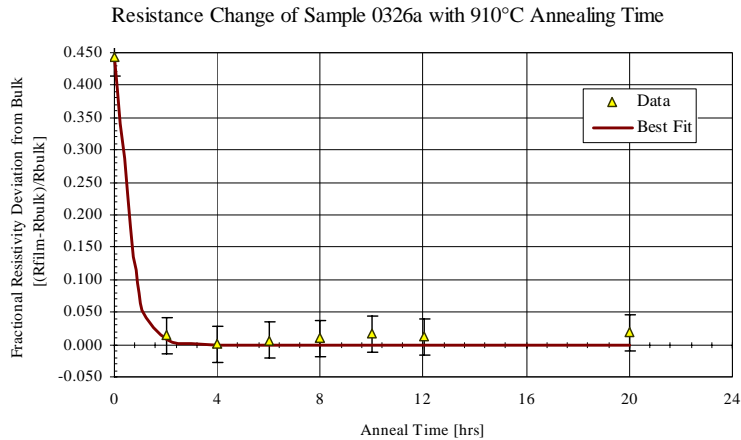


Figure 18.—Resistance change of sample 0326a showing data points and best fit from the developed model.

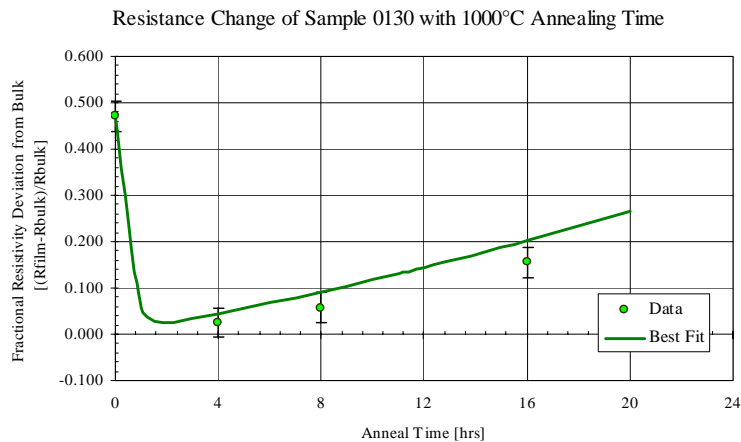


Figure 19.—Resistance change of sample 0130 showing data points and best fit from the developed model.

Annealing the film at 800 °C for 4 hours should be adequate for reduction of the intrinsic strain the film to attain a stability of 0.1 percent and prevent the loss of film. However, if shadowing or flashing of platinum is present and needs to be eliminated, annealing the films at 1000 °C for 3 hours is also acceptable, but the film thickness will be reduced by 0.019 μm, which needs to be taken into account in the sensor design. Using our standard annealing schedule, annealing the films for 4 hours at 1000 °C will result in 0.025 μm film loss, but will further reduce the intrinsic stresses of the films and push the stability to better than 0.02 percent.

The result of 1000 °C annealing was examined on non-patterned films under SEM using samples generated for film adhesion tests below. Figures 20a, 20b, 21a, and 21b show representative pictures of the surfaces. On quartz (figs. 20a and 20b), the as-deposited flat film developed voids and islands after annealing. On alumina (figs. 21a and 21b), a rough film gained a few large voids fairly isolated from each other and large-grained islands scattered about the surface. The islands could be formed from the material that moved from the voids with the increased mobility during annealing, or the islands could be domes of raised grains with voids underneath.

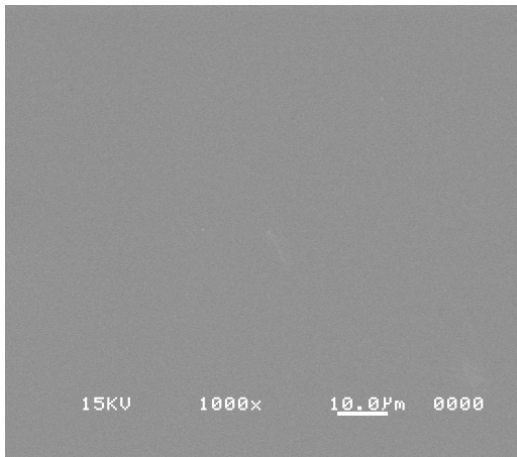


Figure 20a.—Platinum on quartz as-deposited (sample 0401#2 –QZ).
The field of view is 100 µm.

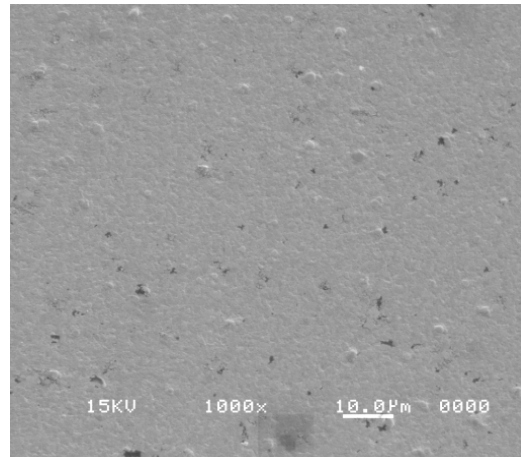


Figure 20b.—Platinum on quartz after 1000 °C anneal (sample 0414#2 –QZ).
The field of view is 100 µm.

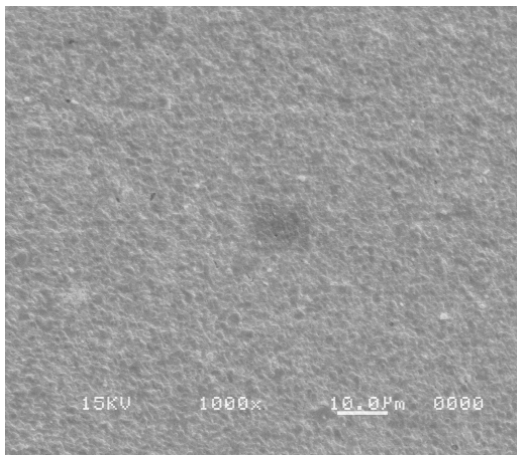


Figure 21a.—Platinum on alumina as-deposited (sample 0401#2 –AO).
The field of view is 100 µm.

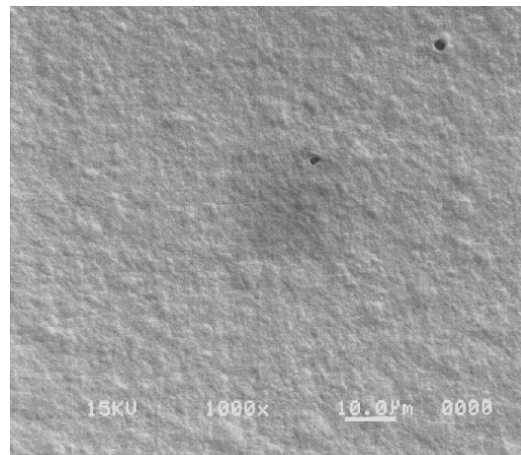


Figure 21b.—Platinum on alumina after 1000 °C anneal (sample 0414#2 –AO).
The field of view is 100 µm.

Film Adhesion

In order to test the adhesion of the platinum films, samples of the films with different platinum oxide bondcoats were fabricated on 1 inch (2.54 cm) square quartz (–QZ) and 1 inch (2.54 cm) square alumina (–AO) substrates, both 0.040 inch (1 mm) thick. The deposition parameters are given in table 6. The film thickness is estimated from the average current and the deposition rate related in the above section. They were annealed for 4 hours in air at 500, 700, and then 1000 °C, in parallel with the annealing studies conducted above.

For all samples in general, surface anomalies increased with each anneal, but no wholesale failures were visible. All films passed a rudimentary “tape test” with transparent tape after each anneal as well. Increasing the amount of oxygen in the bond coat appeared to cause more anomalies and discoloration problems with the platinum films.

A stud-pull test was performed on ¼ inch (6 mm) square pieces cut from each of the samples in table 6. In the stud-pull test, an aluminum stud is exposed perpendicularly to the film on each piece. After curing, the stud is pulled on a mechanical strength tester, the failure pressure along with notations of

substrate failures and stud failures are recorded, and the average failure pressure and standard deviation calculated. A photographic analysis of the film failures determined the area of film detached by the stud as a percentage of total stud area, with the measurement limited by the resolution of the area in the image (± 0.125 percent for the quartz samples, ± 2 percent for the alumina samples). The results are shown in tables 7 and 8.

The studs had better adhesion to the alumina samples than to the fused quartz samples, but the film adhered better to the quartz samples than the alumina samples. As shown in table 7, the average stud failure pressure was $47 \text{ MPa} \pm 10 \text{ MPa}$ for the quartz samples, with multiple substrate failures in the test. The film failure is only apparent for samples 0414#3 and #4 –QZ, and then on average it was less than 2 percent of the total pulling area. It does appear from these tests that the platinum oxide bond coat does not contribute to the adhesion of the films on quartz, and it may be detrimental for oxygen concentrations in the feed gas greater than 10 percent. Attempts to determine the bonding mechanism seen in other sputtered platinum films on quartz by XPS has not revealed any bonding between platinum, the silicon or oxygen, suggesting that the bond is purely mechanical.

For the alumina substrates in table 8, the average stud pull failure was $70 \text{ MPa} \pm 12 \text{ MPa}$. The 0414#2 –AO sample showed the least failure, both in the number of failures and the area of film that failed. In contrast to the quartz substrate samples, the alumina samples indicate better adhesion of the platinum film to the alumina if a bond coat using 10 percent oxygen is utilized. Noting that the adhesion using no oxygen in the deposition was better than the 25 or 50 percent oxygen bond coat films, the optimal mix is suspected to lie somewhere between the 10 percent and the no oxygen mix.

Conclusions

The effort to document the optimal fabrication parameters necessary for the development of high temperature platinum film resistive sensors involved the preparation of samples in a new magnetron sputtering system at NASA Glenn Research Center. The sensors were optimized for system pressure, deposition power and annealing temperature.

The optimal parameters were found to be using a pressure of 5 mTorr with 100 W magnetron power, followed by an annealing cycle of $800 \text{ }^\circ\text{C}$ for 4 hours. At these parameters, the deposition rate is expected to be about $0.82 \text{ } \mu\text{m/hr}$, and may vary based on the actual current. These parameters, outlined in detail in table 9, also can be used as a starting point in optimizing the deposition of similar noble metal films and their alloys, such as palladium or platinum with 13 percent rhodium. The optimization of ceramics such as alumina or silica will be done at a later date.

A film loss model was developed for temperatures above $900 \text{ }^\circ\text{C}$, predicting a loss rate of approximately $62 \text{ } \text{Å/hr}$ at $1000 \text{ }^\circ\text{C}$ and $2500 \text{ } \text{Å/hr}$ at $1500 \text{ }^\circ\text{C}$ through volatile oxidation. The actual rates may be double that. The evaporation, though slight, will affect on the resistance of thin films at these temperatures over time, and with it will come an effective loss of calibration. A protective overcoat to protect the metal from oxidation may be able to extend the useful temperature to over $900 \text{ }^\circ\text{C}$. The film adhesion was also explored. It was found that for platinum films on fused quartz substrates, no adhesion bondcoat was necessary for high temperature applications, but it was for platinum films on alumina substrates. Using the practice of sputtering the platinum in an argon/oxygen atmosphere for bond coat formation indicated an optimal mix of 10 percent oxygen in argon. Comparisons of these results to other high temperature bond coats could be done in the future.

TABLE 6.—MICRO-THIN FILM ADHESION SAMPLES

Sample #	3 min Bond Coat Gas Flow Mix (Ar/O ₂)	1 hr Final Coat Gas Flow Mix (Ar/O ₂)	Average Current (mA) at 100 W	Est. Film Thickness (μm)	Surface appearance (macro)
0414#1 -QZ and -AO	-	40/0	277	0.865	Best looking film after each anneal
0414#2 -QZ and -AO	40/4	40/0	274	0.897	Surface anomalies appeared to decrease after 1000 °C anneal
0414#3 -QZ and -AO	40/10	40/0	273	0.891	Most surface anomalies in general
0414#4 -QZ and -AO	20/20	40/0	269	0.873	Largest increase of surface anomalies after 1000 °C anneal

TABLE 7.—RESULTS OF STUD-PULL ADHESION TESTS OF THE PLATINUM FILMS ON FUSED QUARTZ SUBSTRATES

Sample #	3 min Bond Coat Gas Flow Mix (Ar/O ₂)	Ave. Pressure Stud Failure (MPa)	Test Pieces Surviving (of 8 samples)	Test Pieces Showing Film Failure	Average Area of Film Failure (±0.125%)
0414#1 -QZ	-	53 ± 6	6	0	-
0414#2 -QZ	40/4	48 ± 9	6	1	0.107%
0414#3 -QZ	40/10	46 ± 12	2	1	0.400%
0414#4 -QZ	20/20	43 ± 10	7	3	1.766%

TABLE 8.—RESULTS OF THE STUD-PULL ADHESION TESTS OF PLATINUM FILMS ON ALUMINA SUBSTRATES

Sample #	3 min Bond Coat Gas Flow Mix (Ar/O ₂)	Ave. Pressure Stud Failure (MPa)	Test Pieces Showing Film Failure (of 10 samples)	Average Area of Film Failure (±2%)
0414#1 -AO	-	61 ± 17	80%	13%
0414#2 -AO	40/4	65 ± 12	40%	6%
0414#3 -AO	40/10	85 ± 11	90%	51%
0414#4 -AO	20/20	69 ± 6	100%	58%

TABLE 9.—OPTIMAL PARAMETERS AND CHARACTERISTICS DETERMINED FOR PATTERNED PLATINUM THIN FILMS

Deposition Power	100 WDC
Deposition Pressure	5 mTorr
Bond Coat Gas Mix	Ar/O _x = 40/4
Bond Coat Thickness	300Å/3 minutes
Main Coat Gas Mix	Argon only
Total Deposition Rate	0.82 ± 0.04 μ/hr
Annealing Time and Temperature	4 hrs at 800 °C
Film Uniformity over 2.6 cm	1%–2%
Film Resistivity	10.6 ± 0.4 μOhm-cm

References

1. R.F. Vines, *The Platinum Metals and Their Alloys* (New York, NY: The International Nickel Company, Inc., 1941), 15–33.
2. L.C. Martin and R. Holanda, “Applications of Thin Film Thermocouples for Surface Temperature Measurement,” *Conference on Spin-Off Technologies for Commercial Sensors and Scientific Instrumentation* (San Diego, CA, July 24–29, 1994), NASA TM-106714.
3. G.C. Fralick, J.D. Wrbanek, C.A. Blaha, “Thin Film Heat Flux Sensor of Improved Design,” *48th International Instrumentation Symposium* (San Diego, CA, May 5–9, 2002), NASA/TM—2002-211566.
4. J.D. Wrbanek, G.C. Fralick, L.C. Martin, C.A. Blaha, “A Thin Film Multifunction Sensor for Harsh Environments,” *37th AIAA/ASME/SAE/ASEE Joint Propulsion Conference and Exhibit* (Salt Lake City, UT, July 8–11, 2001), NASA/TM—2001-211075.
5. M. J. Ignatius, N. Sawhney, A. Gupta, B. M. Thibadeau, O. R. Monteiro, I. G. Brown, “Bioactive surface coatings for nanoscale instruments: Effects on CNS neurons,” *J. Biomed. Mater. Res.* 40 (2) (May 1998): 264–274.
6. C.A. Blaha, “Photolithographic Fine Patterning of Difficult-To-Etch Metals,” *NASA Tech Briefs* LEW-17079 (March 2002).
7. R.C. Budhani, S. Prakash, and R.F. Bunshah, “Thin-film sensors for gas turbine engines: Problems and prospects,” *J. Vac. Sci. Technol. A* 4 (6) (Nov./Dec. 1986): 2609–2617.
8. H. Neff, S. Henkel, E. Hartmannsgruber, E. Steinbeiss, W. Michalke, K. Steenbeck, and H. G. Schmidt, “Structural, optical, and electronic properties of magnetron-sputtered platinum oxide films,” *J. Appl. Phys.* 79 (10) (May 1996).
9. D.-S. Lee, D.-Y. Park, M.H. Kim, D.-I. Chun, J. Ha, and E. Yoon, “Characterization of Platinum Films Deposited by a Two-Step Magnetron Sputtering on SiO₂/Si Substrates,” *Thin Films – Structure and Morphology*, S.C. Moss et al. eds., Mat. Res. Soc. Symp. Proc. vol. 441 (1997): 341–346.
10. K. Kuribayashi and S. Kitamura, “Preparation of Pt-PtO_x thin films as electrode for memory capacitors,” *Thin Solid Films* 400 (2001): 160–164.
11. G.F. Strouse, “NIST implementation and realization of the ITS-90 over the range 83 to 1235 K: Reproducibility, stability, and uncertainties,” *Temperature: Its Measurement and Control in Science and Industry*, vol. 6 No. 1, J.F. Schooley, et al. eds. (New York, NY: APS, 1992), 169–178.
12. I. Golecki and M. Eagan, “Influence of the Deposition Parameters on the Electrical and Mechanical Properties of Physically Vapor-Deposited Iridium and Rhodium Thin Films,” *Thin Films – Stresses and Mechanical Properties*, Mat. Res. Soc. Symp. Proc. vol. 594 (2000): 105–110.
13. M. Watanabe, D.R. Mumm, S. Chiras and A.G. Evans, “Measurement of the residual stress in a Pt-aluminide bond coat,” *Scripta Materialia* 46 (2002): 67–70.
14. M.J. Kobrinsky and C.V. Thompson, “Activation Volume for Inelastic Deformation in Polycrystalline Ag Films at Low Temperatures,” *Thin Films – Stresses and Mechanical Properties*, Mat. Res. Soc. Symp. Proc. vol. 594 (2000): 57–62.
15. C.B. Alcock and G.W. Hooper, “Thermodynamics of the gaseous oxides of the platinum-group metals,” *Phys. Roy. Soc. A* 254 (1960): 551–561.
16. S.E. Schwartz, “Historical Perspective on Heterogeneous Gas-Particle Interaction,” *Mass Accommodation Workshop* (Billerica, MA, February 25–28, 2002). http://www.ecd.bnl.gov/steve/Hist_Persp_Het.pdf (August 2003).
17. W.H. Bennethum and L.T. Sherwood, *Sensors for Ceramic Components in Advanced Propulsion Systems*, NASA CR-180900 (GE Aircraft Engines, August 1988), 7–8.

REPORT DOCUMENTATION PAGE

Form Approved
OMB No. 0704-0188

Public reporting burden for this collection of information is estimated to average 1 hour per response, including the time for reviewing instructions, searching existing data sources, gathering and maintaining the data needed, and completing and reviewing the collection of information. Send comments regarding this burden estimate or any other aspect of this collection of information, including suggestions for reducing this burden, to Washington Headquarters Services, Directorate for Information Operations and Reports, 1215 Jefferson Davis Highway, Suite 1204, Arlington, VA 22202-4302, and to the Office of Management and Budget, Paperwork Reduction Project (0704-0188), Washington, DC 20503.

1. AGENCY USE ONLY <i>(Leave blank)</i>		2. REPORT DATE January 2005	3. REPORT TYPE AND DATES COVERED Technical Memorandum	
4. TITLE AND SUBTITLE Preparation and Analysis of Platinum Thin Films for High Temperature Sensor Applications			5. FUNDING NUMBERS WBS-22-794-20-5E	
6. AUTHOR(S) John D. Wrbanek and Kimala L.H. Laster				
7. PERFORMING ORGANIZATION NAME(S) AND ADDRESS(ES) National Aeronautics and Space Administration John H. Glenn Research Center at Lewis Field Cleveland, Ohio 44135-3191			8. PERFORMING ORGANIZATION REPORT NUMBER E-14967	
9. SPONSORING/MONITORING AGENCY NAME(S) AND ADDRESS(ES) National Aeronautics and Space Administration Washington, DC 20546-0001			10. SPONSORING/MONITORING AGENCY REPORT NUMBER NASA TM-2005-213433	
11. SUPPLEMENTARY NOTES John D. Wrbanek, NASA Glenn Research Center; and Kimala L.H. Laster, Akima Corporation, Brook Park, Ohio 44142. Responsible person, John D. Wrbanek, organization code RIS, 216-433-2077.				
12a. DISTRIBUTION/AVAILABILITY STATEMENT Unclassified - Unlimited Subject Category: 35 Available electronically at http://gltrs.grc.nasa.gov This publication is available from the NASA Center for AeroSpace Information, 301-621-0390.			12b. DISTRIBUTION CODE	
13. ABSTRACT <i>(Maximum 200 words)</i> A study has been made of platinum thin films for application as high temperature resistive sensors. To support NASA Glenn Research Center's high temperature thin film sensor effort, a magnetron sputtering system was installed recently in the GRC Microsystems Fabrication Clean Room Facility. Several samples of platinum films were prepared using various system parameters to establish run conditions. These films were characterized with the intended application of being used as resistive sensing elements, either for temperature or strain measurement. The resistances of several patterned sensors were monitored to document the effect of changes in parameters of deposition and annealing. The parameters were optimized for uniformity and intrinsic strain. The evaporation of platinum via oxidation during annealing over 900 °C was documented, and a model for the process developed. The film adhesion was explored on films annealed to 1000 °C with various bondcoats on fused quartz and alumina. From this compiled data, a list of optimal parameters and characteristics determined for patterned platinum thin films is given.				
14. SUBJECT TERMS Thin films; High temperature sensors; Magnetron sputtering; Platinum; Annealing			15. NUMBER OF PAGES 25	
			16. PRICE CODE	
17. SECURITY CLASSIFICATION OF REPORT Unclassified	18. SECURITY CLASSIFICATION OF THIS PAGE Unclassified	19. SECURITY CLASSIFICATION OF ABSTRACT Unclassified	20. LIMITATION OF ABSTRACT	

